Characterization of Novel Varistor+Inductor Integrated Passive Devices

Ramesh Raghavendra, Pat Bellew, Neil Mcloughlin, Goran Stojanovic, *Student Member, IEEE*,
Mirjana Damnjanovic, *Student Member, IEEE*, Vladan Desnica, *Member, IEEE*, and Ljiljana Zivanov, *Member, IEEE*

Abstract—This letter describes the design, modeling, simulation, and fabrication of novel integrated passive devices (IPDs). These IPDs, comprising of a cofired multilayered varistor and inductor, have been developed in the ceramic coprocessing technology. The equivalent model of the new structures is presented, suitable for design and circuit simulations. The fabrication method, new design of structures and patented materials of these devices lead to improved characteristics suitable for application in high-frequency suppressors. The IPDs were tested in the frequency range of 1 MHz–3 GHz using an Agilent 4287A RF LCR meter. The measurements confirm the validity of the proposed model.

Index Terms—Coils, high-frequency suppression, integrated passive devices, surface mounted devices, varistor.

I. INTRODUCTION

THE CONCEPT of integrated passive devices (IPDs) involves manufacturing the passives as a group in or on a common substrate, instead of in their own individual packages [1]. Commercial off-the-shelf passive components such as resistors, capacitors, inductors, or varistors are an integral part of every electronic subsystem present on todays market [2]. The advantages of IPDs are numerous, such as smaller system size, better electrical performance, and improved system reliability. The improvement in parasitics leads to an increase in the operating frequency range when compared to discrete passive components. In addition, each integrated passive eliminates solder joints, which translates to improved reliability. When comparing discrete varistor and inductor devices with integrated varistor+inductor (VarInd) ones, a reduction of real estate of least 50% has been achieved. The protection of devices from damage can be achieved using zinc oxide-based varistors, which provide transient protection and are very effective in suppressing high amplitude and low-frequency transients. Inductors, also, can be used as a protection against electromagnetic interference (EMI). IPDs are devices having more than one function (e.g., capacitor+inductor or varistor+inductor) formed within a single common substrate or package and thus replace multiple passive components [3]–[5]. The characterization and modeling of inductors with a ferrite core and varistor, as discrete components, have been discussed
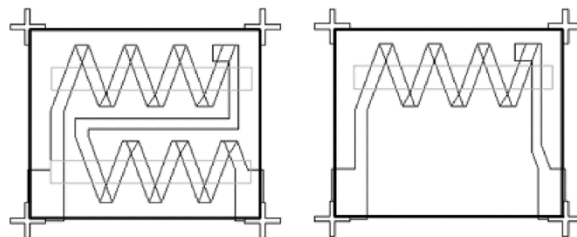
Fig. 1. Layout of double and single coil (with varistor core) structures.
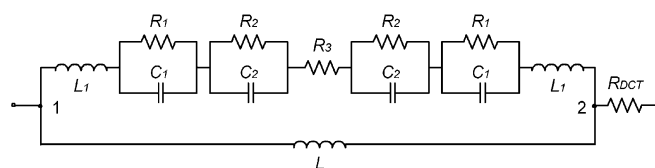
Fig. 2. Equivalent circuit of varistor+inductor structure.

in available literature [6]–[11]. The electrical model and characterization of complex coil structures embedded in varistor material over a wide frequency range has not been reported yet. In this letter the new design, modeling and fabrication of single and double coils, with a varistor core embedded in the varistor material, are described.

II. PHYSICAL DESCRIPTION AND MODELING OF IPDs

The proposed novel VarInd structures are realized as surface-mount devices for the typical 1210 chip size. Layouts of a double coil and single coil (with varistor core) are depicted in Fig. 1. The components have been fabricated using the ceramic coprocessing technology. Varistor paste V26-1210 was used [4]. Platinum (Pt) was chosen as the conductor to form the single and double coils. The coils are embedded in the middle of a varistor layer (2.87 mm thick) and the core is made from a varistor layer 18 μm thick. The chosen varistor formulation is composed primarily of zinc oxide, with small additions of bismuth, cobalt, manganese, and other metal oxides.

In order to analyze single and double coils with a varistor core and embedded in varistor material, the equivalent circuit, describing electrical properties of presented structure, is determined and is depicted in Fig. 2. In the first step, for the varistors part, three blocks are considered for the equivalent circuit, similarly as in [11]. These are a grain boundary layer, a depletion layer, and a conduction layer. In the conduction layer, only resistance is considered (R_3), while in the grain boundary and depletion layers, a parallel circuit composed of a resistance and a capacitance is considered $(R_1 \| C_1$, and $R_2 \| C_2)$. In the second

step, we modeled the inductor's part. L_1 is a very small inductance toward the electrodes, while L represents the total inductance of a single or double coil. We have developed a logical combination of the two models [9], [11] with the addition of some elements in order to obtain better agreement between simulated and experimental data.

Simulations of single and double coils embedded in varistor material were performed using our software tool—simulator for planar inductive structures (SPIS) based on the calculation method described briefly in this subsection. The coil is divided into segments having small, rectangular cross sections. The total inductance of the single and double coils is calculated using the Greenhouse method [12]. To obtain the correct total inductance L, the mutual inductance M between all segments of the inductor has to be calculated and added to the sum of all segments self-inductance $L_S (L = \sum L_S + \sum M)$. The computation concept of mutual inductance among the coils considers segments as simple filaments. The mutual inductance M of two straight segments placed in any desired position is calculated by means of formulas as in [13, p. 56].

The extraction of other equivalent circuit parameters was done using a fitting procedure according to the measured data and the components physical characteristics.

If the equivalent impedance of the circuit shown in Fig. 2 (between 1 and 2) is defined as $Z_{\rm eq}$, then the effective inductance can be calculated as $L_{\rm eff} = (\text{Im}(Z_{\rm eq}))/(2 \cdot \pi \cdot f)$, where f is frequency. The effective resistance can be calculated as $R_{\rm eff} = R_{\rm DCT} + \text{Re}(Z_{\rm eq})$. The total dc resistance $R_{\rm DCT}$ (shown in Fig. 2) is several times larger (due to the resistance of the contacts) than the resistance calculated by $R_{\rm dc} = (\rho - l)/(w \cdot t)$, where ρ is resistivity of a Pt conductor layer of a thickness t, width w and total length l. Therefore, the effective impedance and the quality factor of the VarInd are determined by $Z_{\rm eff} = \sqrt{R_{\rm eff}^2 + (\text{Im}(Z_{\rm eq}))^2}$, and $Q = (\text{Im}(Z_{\rm eq}))/(R_{\rm eff})$.

As an illustration, values of the model parameters, for a single coil, at frequency of 1 GHz are: $R_1 = 15\ \Omega, R_2 = 1000\ \Omega, R_3 = 4\ \Omega, C_1 = 20$ pF, $C_2 = 30$ pF, L = 2.81 nH, $L_1 = 0.3$ pH. For these values of model parameters, the following electrical parameters are obtained: $L_{\rm eff} = 4.68$ nH, $R_{\rm eff} = 28.97\ \Omega, Z_{\rm eff} = 41.31\ \Omega$ and $Q = 1.02$. The proposed model allows accurate prediction of all the parameters affecting the VarInd, as well as their control during the design process.

III. RESULTS AND DISCUSSION

The measurement and characterization of the components have been performed using an Agilent 4287A RF LCR meter for frequencies up to 3 GHz. Electrical data obtained for the components, proposed in Fig. 1, are shown in Figs. 3 and 4. The resistance and inductance versus frequency are plotted in Fig. 3(a), and (b), while the impedance and Q-factor versus frequency are plotted in Fig. 4(a), and (b), respectively. The inset in Fig. 4(a) includes the impedance characteristics of a commercial component, SurgeCap (varistor+capacitor IPD, V26MVC-1210). The impedance curve of VarInd IPD is inverse to the curve of SurgeCap IPD [4].

Results have shown that the single coil demonstrates better characteristics than the double coil, especially at higher frequen-
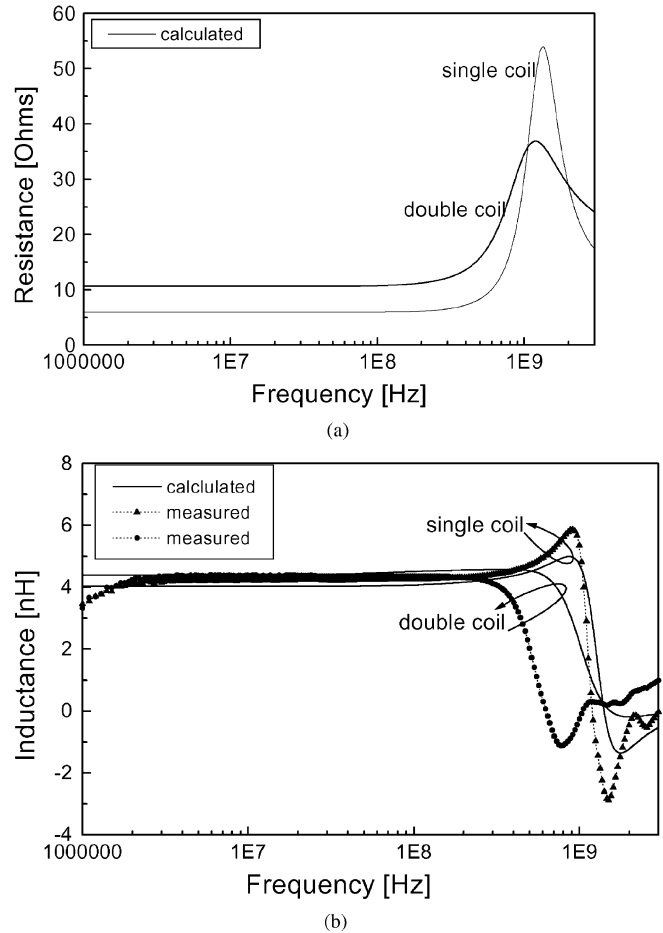

Fig. 3. (a) Calculated effective resistance, and (b) measured and calculated effective inductance.

cies (it has about a $65/5$ impedance ratio). The double coil has greater values of resistance and impedance at lower frequencies. Double resonance is noticed, clearly visible in Fig. 4(b) in the measured data. This results from separate parasitic inductances associated with the varistor and inductor elements, and it is a feature that can be usefully exploited for decoupling applications. The quality factor shows local maxima at frequencies below 1 GHz, thus lending the structure to usage in this frequency range.

Cofiring of ceramics is not easy and is fraught with difficulty. Material diffusion or contamination is a key concern when dealing with electrical properties [14]. The diffusion of Pt into the varistor material can result in deterioration of both the varistor material and the conductor material characteristics. It is not possible to include this phenomenon in the model successfully. Thus, the deviation of the measurement results compared to the calculated ones in the range of about 1 GHz is a consequence of the above reasons, and this deviation is greater in the case of a double coil.

The proposed structures proved to have the expected advantages such as increased circuit density achieved by the reduced footprint, cost reduction due to the reduction of component number on board surface, increased product quality through the elimination of incorrectly attached devices, and improved reliability through the elimination of solder joints.
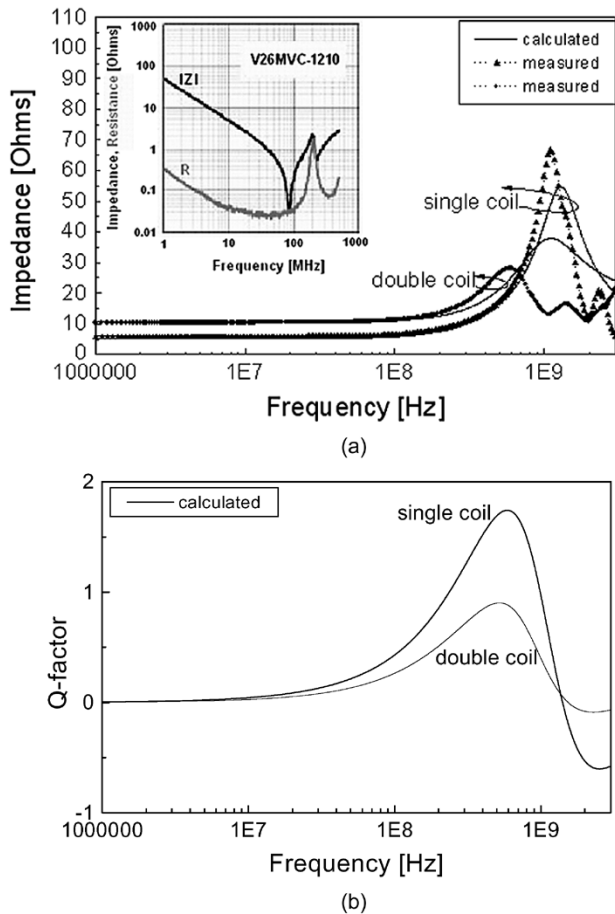
Fig. 4.   (a) Measured and calculated effective impedance, and (b) calculated quality factor. The inset in Fig. 4(a) shows the impedance characteristics of a commercial component, SurgeCap (varistor+capacitor IPD, V26MVC-1210).

IV. CONCLUSION

The new presented components have enhanced EMI suppression capabilities over equivalent standard discrete components. In addition, these cofired devices possess better clamping of fast transients, such as electrostatic discharge. Potential applications for the proposed VarInd IPDs include bandstop filters, power rail decoupling with added surge suppression, low data-rate signal circuits and filter element replacement. VarInd components would have an average unit price of the same order as commercial off-the-shelf discrete components with similar applications and a much smaller occupied area (at least 50%). The results obtained by the proposed method are in good agreement with the measured data.

REFERENCES

[1]   J. P. Dougherty, "Integrated passives technology and economics," *Circuits Assem.*, pp. 18–23, Sept. 2003.
[2]   M. Scheffler, G. Troster, J. L. Contreras, J. Hartung, and M. Menard, "Assessing the cost-effectiveness of integrated passives," *Microelectron. Int.*, vol. 17/3, pp. 11–15, 2000.
[3]   O. Aleksić, P. Nikolić, M. Luković, and D. Vasiljević-Radović, "Planar thick film integrated LCV cells," *Microelectron. Int.*, no. 38, pp. 12–15, Sept. 1995.
[4]   R. Raghavendra, P. Bellew, and N. Mcloughlin, "Coprocessing of electroceramics technology: A simple IPD for combined transient & EMI suppression applications," *Passive Comp. Ind.*, pp. 13–17, Jan./Feb. 2002.
[5]   V. Desnica, Lj. Živanov, O. Aleksić, M. Luković, and M. Nimrihter, "A comparative characteristics of thick film integrated LC filters," *IEEE Trans. Instrum. Meas.*, vol. 51, pp. 570–576, Aug. 2002.
[6]   J. Y. Hsu, H. Ch. Lin, H. D. Shen, and Ch. J. Chen, "High frequency multilayer chip inductors," *IEEE Trans. Magn.*, vol. 33, no. 5, pp. 3325–3327, Sept. 1997.
[7]   M. K. Kazimierczuk, G. Sancineto, G. Grandi, U. Reggiani, and A. Massarini, "High-frequency small-signal model of ferrite core inductors," *IEEE Trans. Magn.*, vol. 35, no. 5, pp. 4185–4191, Sept. 1999.
[8]   M. Bartoli, A. Reatti, and M. K. Kazimierczuk, "Modeling iron-powder inductors at high frequencies," in *Proc. IEEE Industry Applications Society Annual Meeting*, Oct. 1994, pp. 1225–1232.
[9]   A. Massarini and M. K. Kazimierczuk, "Self-capacitance of inductors," *IEEE Trans. Power Electron.*, vol. 12, pp. 671–676, July 1997.
[10] A. Reatti and M. K. Kazimierczuk, "Comparison of various methods for calculating the AC resistance of inductors," *IEEE Trans. Magn.*, vol. 38, pp. 1512–1518, May 2002.
[11] S. W. Han, H. B. Kang, and H. S. Kim, "Effects of aluminum as dopants on the AC impedance and J-E behavior of $ZnO-Bi_2O_3$ ceramics," in *Proc. 5th Int. Conf. Properties Applications Dielectric Materials*, Seoul, Korea, May 25–30, 1997, pp. 863–866.
[12] H. M. Greenhouse, "Design of planar rectangular microelectronic inductors," *IEEE Trans. Parts, Hybrids, Packag.*, vol. PHP-10, pp. 101–109, June 1974.
[13] F. W. Grover, *Inductance Calculations, Working Formulas and Tables*.   New York: Van Nostrand, 1946.
[14] A. Rafferty, Y. Gun'ko, and R. Raghavendra, "An investigation of co-fired varistor-ferrite materials," *J. Eur. Ceramic Soc.*, vol. 24, no. 7, pp. 2005–2013, June 2004.